International Journal of Multiphase Flow xxx (2009) xxx–xxx

Contents lists available at ScienceDirect

International Journal of Multiphase Flow

journal homepage: www.elsevier.com/locate/ijmulflow

Review

Physics and modelling of turbulent particle deposition and entrainment: Review of a systematic study

Alfredo Soldati *, Cristian Marchioli

Dipartimento di Energetica e Macchine and Centro Interdipartimentale di Fluidodinamica e Idraulica, Università degli Studi di Udine, Udine, Italy

ARTICLE INFO

Article history:
Received 1 July 2008
Received in revised form 16 February 2009
Accepted 19 February 2009
Available online xxxx

Keywords:
Turbulent boundary layer
Coherent structures
Particle dispersion
Direct numerical simulation
Lagrangian particle tracking

ABSTRACT

Deposition and entrainment of particles in turbulent flows are crucial in a number of technological applications and environmental processes. We present a review of recent results from our previous works, which led to physical insights on these phenomena. These results were obtained from a systematic numerical study based on the accurate resolution – Direct Numerical Simulation via a pseudo-spectral approach – of the turbulent flow field, and on Lagrangian tracking of particles under different modelling assumptions. We underline the multiscale aspect of wall turbulence, which has challenged scientists to devise simple theoretical models adequate to fit experimental data, and we show that a sound rendering of wall turbulence mechanisms is required to produce a physical understanding of particle deposition and re-entrainment. This physical understanding can be implemented in more applied simulation techniques, such as Large-Eddy Simulation. Our arguments are based also on the phenomenology of coherent structures and on the examination of flow topology in connection with particle preferential distribution. Starting from these concepts, reasons why theoretical predictions may fail are examined together with the requirements which must be fulfilled by suitable predictive models.

1. Introduction

In the context of turbulent dispersed flows (gas–solid, gas–liquid and liquid–solid), a key information for practical applications is the rate at which the dispersed phase (e.g. particles, droplets and aerosols; from now on referred to as particles for sake of simplicity) is transported to, deposited at, and re-entrained from a solid boundary by turbulence. In relation to the many and complex phenomena involved, an elemental physical insight was given by Friedlander and Johnstone (1957) in their early paper: the "*rate of particle transfer is always less than or equal to the transfer rate of the common gases which follow approximately the Reynolds analogy*". This remark provides the essentials for a model: first it is necessary to understand wall turbulence, second it is necessary to understand the coherent flow motions (instantaneous realizations of the Reynolds stresses), and third it is necessary to model the intrinsic inadequacy of the adverb *approximately* both in qualitative terms – phenomena – and quantitative terms – models. A number of later studies had emerged to investigate on the same problem, but it is beyond the scope of this paper to make a complete literature review; rather we just cite a few experimental studies (among others: Kaftori et al., 1995a,b; Niño and Garcia, 1996) and theoretical developments (from Caporaloni et al., 1975; Cleaver and Yates, 1975; to Cerbelli et al., 2001; Slater et al., 2003). Upon examination of most of the published works, it emerges that the main difficulty of the modelling approaches is associated with the inability of particles to follow turbulent vortices: due to inertia, they cross through vortices and accumulate into specific flow regions where they tend to stay long time. For this reason, particles do not experience fully the Eulerian statistics of the turbulent flow field; rather they sample it only preferentially (see Fessler et al., 1994; and references therein). The response to a lack of satisfactory theories produced an effort to collect experimental data sources for model benchmarking: examples, mostly referring to fully-developed turbulent flow in straight vertical tubes or ducts, can be retrieved in the paper by Young and Leeming (1997) or, more recently, in the report by Sippola and Nazaroff (2002). An interesting feature of these data collections is the inaccuracy affecting measurements in the so-called "diffusion–impaction" regime. In this regime, particles are large enough for their inertia to be influential on their motion and small enough to become rather quickly independent of the strong motions characterizing the regions away from the walls. In fact, the inertia of these particles is just but sufficient to influence their motion in the wall region.

In our previous papers (Marchioli and Soldati, 2002; Marchioli et al., 2003, 2006; Picciotto et al., 2005) it was shown that there is a strong correlation between coherent wall structures, local particle segregation and subsequent deposition phenomena, which have been subdivided into several steps, all quantified from a statistical viewpoint. Specifically, it was demonstrated that, in the dif-

* Corresponding author. Tel.: +39 0432 558020.
E-mail address: soldati@uniud.it (A. Soldati).

0301-9322/$ - see front matter © 2009 Elsevier Ltd. All rights reserved.
doi:10.1016/j.ijmultiphaseflow.2009.02.016

Please cite this article in press as: Soldati, A., Marchioli, C. Physics and modelling of turbulent particle deposition and entrainment: Review of a systematic study. Int. J. Multiphase Flow (2009), doi:10.1016/j.ijmultiphaseflow.2009.02.016

fusion–impaction regime, particles deposition process is initially dominated by inertia-induced segregation and accumulation into specific flow regions close to the walls. Only afterwards particles are driven to the walls. Modelling this physical mechanism is non-trivial, especially with numerical methods coarser than DNS. The complicacy lies in the complex interaction between particle inertia and the non-homogeneous structure of turbulence in the wall-normal direction and justifies the lack of physically-based accurate correlations for particle deposition flux (Oliemans et al., 1986; Soldati and Andreussi, 1996).

In this paper, we will review the most relevant findings obtained at our computational laboratory through systematic investigation of particles–turbulence interaction in boundary layer by means of Eulerian–Lagrangian numerical simulations. Specifically, we will refer to Direct Numerical Simulations (DNS) and complementary Large-Eddy Simulations (LES) of fully-developed gas–solid channel flow under the pointwise particle approximation. Also, we will focus on particles which possess inertia, emphasizing results more than techniques. Despite the limitations to the modelling capabilities introduced by the point-particle approximation, this approach can still provide the proper level of description to extract physical knowledge from a complex two-phase system. According to our experience, this approach is fully representative of the main qualitative features characterizing particles–turbulence interaction in boundary layer in the limit of *small* particles and dilute flow conditions.

The paper is organized as follows. First, we will describe the numerical methodology (Section 2). Then, we will overview the mechanisms by which particles are deposited at the wall, trapped inside the boundary layer and entrained into the outer flow region (Section 3). Finally we will review the statistical tools that can be used to quantify and characterize these phenomena, also identifying current limitations of LES and possible lines of development (Section 4).

2. Physical modelling and numerical methodology

The reference geometry consists of two infinite flat parallel walls: the origin of the coordinate system is located at the center of the channel and the x, y and z axes represent streamwise, spanwise and wall-normal directions, respectively (see Fig. 1). Periodic boundary conditions are imposed on the fluid velocity field in the homogeneous directions (x and y), no-slip boundary conditions are imposed at the walls ($z = -h$ and $z = h$ in Fig. 1). The size of the computational domain is $L_x \times L_y \times L_z = 4\pi h \times 2\pi h \times 2h$. We consider non-reactive, isothermal and incompressible (low Mach number) flow and monodispersed micrometer-size particles. Calculations are done using variables in dimensionless, represented by the superscript + and expressed in wall units, but to focus on application we consider air with density $\rho = 1.3\ \mathrm{kg\ m^{-3}}$ and kinematic viscosity $\nu = 15.7 \times 10^{-6}\ \mathrm{m^2\ s^{-1}}$, and pointwise heavy particles with density $\rho_p = 10^3\ \mathrm{kg\ m^{-3}}$ and diameters ranging from 10 to 100μm (see Tables 1 and 2).

2.1. Equations for the fluid phase and flow solver

For the DNS, the governing balance equations for the fluid in dimensionless form read as (Soldati and Banerjee, 1998; Soldati, 2000):

$$\frac{\partial u_i}{\partial x_i} = 0, \tag{1}$$

$$\frac{\partial u_i}{\partial t} = -u_j \frac{\partial u_i}{\partial x_j} + \frac{1}{Re_\tau} \frac{\partial^2 u_i}{\partial x_j^2} - \frac{\partial p}{\partial x_i} + \delta_{1,i}, \tag{2}$$

where u_i is the ith component of the velocity vector, p is the fluctuating kinematic pressure, $\delta_{1,i}$ is the mean pressure gradient that drives the flow and $Re_\tau \equiv u_\tau h/\nu$ is the Reynolds number based on the shear (or friction) velocity, u_τ, and on the half channel height, h. The shear velocity is $u_\tau \equiv \sqrt{\tau_w/\rho}$, where τ_w is the mean shear stress at the wall. The superscript + is dropped from Eqs. (1) and (2) for ease of reading.

For the LES, the governing balance equations are smoothed with a filter function of width Δ. Accordingly, all flow variables are decomposed into a resolved (large-scale) part and a residual (subgrid scale) part as $\mathbf{u}(\mathbf{x}, t) = \bar{\mathbf{u}}(\mathbf{x}, t) + \delta\mathbf{u}(\mathbf{x}, t)$. The filtered equations for the resolved scales are then:

$$\frac{\partial \bar{u}_i}{\partial x_j} = 0, \tag{3}$$

$$\frac{\partial \bar{u}_i}{\partial t} = -\bar{u}_j \frac{\partial \bar{u}_i}{\partial x_j} + \frac{1}{Re_\tau} \frac{\partial^2 \bar{u}_i}{\partial x_j^2} - \frac{\partial \bar{p}}{\partial x_i} + \delta_{1,i} - \frac{\partial \tau_{ij}}{\partial x_j}, \tag{4}$$

where $\tau_{ij} = \overline{u_i u_j} - \bar{u}_i \bar{u}_j$ represents the subgrid scale (SGS) stress tensor. The large-eddy dynamics is closed once a model for τ_{ij} is provided. In our studies, the dynamic SGS model of Germano et al. (1991) was adopted.

The flow solver used to perform the numerical simulations is based on a pseudo-spectral method that transforms the field variables into wave space to discretize the governing equations. In the homogeneous directions (x and y), all the quantities are expressed by Fourier expansions using k_x and k_y wavenumbers. In the wall-normal non-homogeneous direction, they are represented by Chebyshev polynomials. The solution, represented spectrally in all three flow directions, has the general form:

$$\mathbf{u}(k_x, k_y, n) = \sum_{k_x} \sum_{k_x} \sum_{n} \hat{\mathbf{u}}(k_x, k_y, n) e^{i(k_x x + k_y y)} T_n(z), \tag{5}$$

in which $T_n(z) \equiv \cos[n \cdot \cos^{-1}(z/h)]$ is the nth order Chebyshev polynomial. By using the orthogonality property of $e^{i(k_x x + k_y y)}$, the equations for the Fourier coefficients $\hat{\mathbf{u}}(k_x, k_y, n)$ can be obtained. All the differential equations to be solved are of Helmholtz type with Dirichlet boundary conditions specified at the walls. Equations are time advanced using a two-level explicit Adams–Bashforth scheme for the non-linear convection terms and an implicit Crank–Nicolson method for the diffusion terms. All calculations are carried out in wave space except for the non-linear terms, which are computed in the physical space and then transformed back to wave space. This numerical scheme is standard for direct simulation of turbulence in domains of simple geometry, such as rectangular channels (Soldati and Banerjee, 1998; Soldati, 2000).

2.2. Equations for the dispersed phase and Lagrangian particle tracking

In the Lagrangian framework, the motion of particles is described by a set of ordinary differential equations for particle position, $\mathbf{x}_p$, and velocity, $\mathbf{u}_p$. These equations in vector form read as:

$$\frac{d\mathbf{x}_p}{dt} = \mathbf{u}_p, \tag{6}$$

$$\frac{d\mathbf{u}_p}{dt} = \frac{(\mathbf{u}_{@p} - \mathbf{u}_p)}{\tau_p}(1 + 0.15 Re_p^{0.687}), \tag{7}$$

where $\mathbf{u}_{@p}$ is the fluid velocity at the particle position, and $\tau_p \equiv \rho_p d_p^2/18\mu$ is the particle relaxation time (d_p and μ being the diameter of the particle and the dynamic viscosity of the fluid, respectively). The Stokes drag coefficient is computed using a standard non-linear correction required when the particle Reynolds number, $Re_p = |\mathbf{u}_{@p} - \mathbf{u}_p| d_p/\nu$, does not remain small (i.e. sufficiently large inertia).

Please cite this article in press as: Soldati, A., Marchioli, C. Physics and modelling of turbulent particle deposition and entrainment: Review of a systematic study. Int. J. Multiphase Flow (2009), doi:10.1016/j.ijmultiphaseflow.2009.02.016

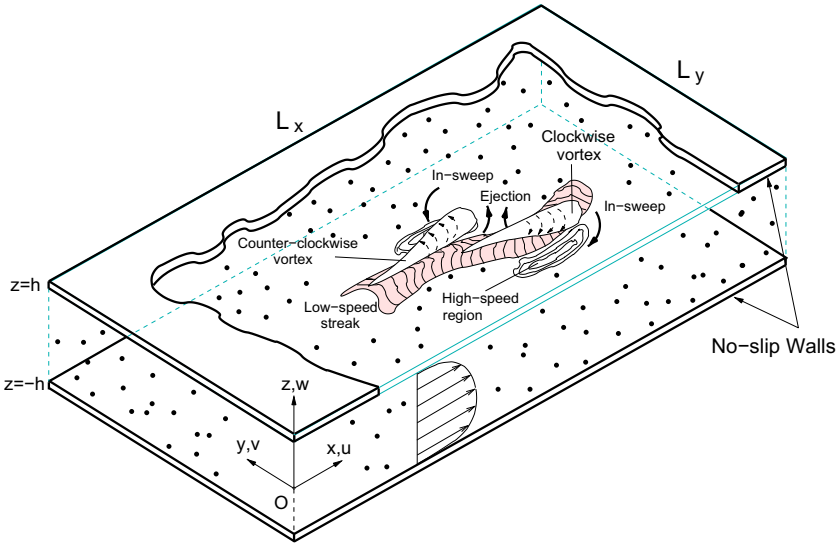

Fig. 1. Particle-laden turbulent gas flow in a channel: sketch of the computational domain and minimal schematics of near-wall turbulent coherent structures. Strong causal relationship links low-speed streaks to ejections generated by quasi-streamwise vortices, which also generate in-sweeps of high streamwise momentum fluid to the wall in the high velocity regions.

Table 1
Particle parameters for the Re_τ^l direct numerical simulations.

$St^l = St\|_{Re_\tau^l}$	τ_p^l (s)	d_p^+	d_p (μm)	$V_s^+ = g^+ \cdot St$	$Re_p^+ = V_s^+ \cdot d_p^+ / \nu^+$
0.2	0.227×10^{-3}	0.068	9.1	0.0188	0.00128
1	1.133×10^{-3}	0.153	20.4	0.0943	0.01443
5	5.660×10^{-3}	0.342	45.6	0.4717	0.16132
25	28.32×10^{-3}	0.765	102.0	2.3584	1.80418
125	1.415×10^{-1}	1.71	228	11.792	20.1643

Table 2
Particle parameters for the Re_τ^h direct numerical simulations.

$St^h = St\|_{Re_\tau^h}$	τ_p^h (s)	d_p^+	d_p (μm)	$V_s^+ = g^+ \cdot St$	$Re_p^+ = V_s^+ \cdot d_p^+ / \nu^+$
1	0.283×10^{-3}	0.153	10.2	0.0118	0.00275
4	1.132×10^{-3}	0.306	20.4	0.0472	0.01444
5	1.415×10^{-3}	0.342	22.8	0.0590	0.02018
20	5.660×10^{-3}	0.684	45.6	0.2358	0.16129
25	7.075×10^{-3}	0.765	51.0	0.2948	0.22552
100	28.30×10^{-3}	1.530	102.0	1.1792	1.80418

To calculate individual particle trajectories, a Lagrangian tracking routine is coupled to the DNS/LES flow solver. The routine solves for Eqs. (7) and (6) under the following assumptions: (i) particles are pointwise, non-rotating rigid spheres (point-particle approach); (ii) particles are injected into the flow at concentration low enough to consider dilute system conditions: the effect of particles onto the turbulent field is neglected (one-way coupling approach) as well as inter-particle collisions. The equations of particle motion are time advanced by a 4th-order Runge–Kutta scheme: at the beginning, particles are randomly distributed over the computational domain and their initial velocity is set equal to that of the fluid at the particle initial position. In our study, fluid velocity interpolation is performed using 6th-order Lagrangian polynomials (near the wall, the interpolation scheme switches to one-sided). The timestep for particle tracking was chosen equal to that of the fluid, $\delta t^+ = 0.045$, more than four times smaller than the non-dimensional response time of the smallest particle tracked ($St^l = 0.2$) and fully adequate to represent precisely particle dynamics (Marchioli et al., 2008c). Periodic boundary conditions are imposed on particles moving outside the computational domain in the homogeneous directions. Eq. (7) does not include near-wall hydrodynamic effects which may complicate the actual mechanism of deposition when the particle-to-wall distance becomes small compared to particle size: perfectly-elastic collisions at the smooth walls are assumed when the particle center is at a distance lower than one particle radius from the wall (Marchioli and Soldati, 2002).

For the purposes of performing a phenomenological study of turbulent particle dispersion and investigating the fundamental physics of the deposition and entrainment phenomena, a base simulation was undertaken in which the setting is kept as simplified as possible and the number of degrees of freedom is minimized. Subsequent inclusion of additional forces (gravity and lift in our problem) can be added to single out their specific effect on particles and to analyze possible changes to the physical scenario depicted by the base simulation. However, several previous works (Marchioli and Soldati, 2002; Arcen et al., 2006; Marchioli et al., 2007) have demonstrated that, within the range of parameters examined – particle dimension (see Tables 1 and 2 for details), density, and concentration – the effect of these forces just adds quantitative corrections (Marchioli and Soldati, 2002; Arcen et al., 2006; Marchioli et al., 2007). In the limit of the dilute flow assumption, the two-way coupling – particles feedback onto the flow field – will also add just quantitative corrections and the weak modulation of the flow (Kaftori et al., 1995a,b; Pan and Banerjee, 1996) will not modify substantially the quality of the model (Soldati, 2005).

2.3. Database and repositories

The results presented in this paper are relative to two values of the Reynolds number: $Re_\tau = 150$ (Re_τ^l hereinafter) corresponding to a shear velocity $u_\tau^l = 0.11775$ ms^{-1}, and $Re_\tau = 300$ (Re_τ^h hereinafter) corresponding to a shear velocity $u_\tau^h = 0.2355$ ms^{-1}. Average (bulk) Reynolds numbers are thus $Re_b^l \equiv u_b^l h/\nu = 2100$, where $u_b^l \simeq 1.65$ ms^{-1} is the average (bulk) velocity; and $Re_b^h \equiv u_b^h h/\nu = 4200$, where $u_b^h \simeq 3.3$ ms^{-1}, respectively. The size of the computational

Please cite this article in press as: Soldati, A., Marchioli, C. Physics and modelling of turbulent particle deposition and entrainment: Review of a systematic study. Int. J. Multiphase Flow (2009), doi:10.1016/j.ijmultiphaseflow.2009.02.016

domain in wall units is $L_x^+ \times L_y^+ \times L_z^+ = 1885 \times 942 \times 300$ for the Re_τ^l simulations and $L_x^+ \times L_y^+ \times L_z^+ = 3770 \times 1885 \times 600$ for the Re_τ^h simulations. In DNS, the computational domain was discretized in physical space with $128 \times 128 \times 129$ grid points (128×128 Fourier modes and 129 Chebyshev coefficients in the wave space) for the Re_τ^l simulations and with $256 \times 256 \times 257$ grid points (256×256 Fourier modes and 257 Chebyshev coefficients in the wave space) for the Re_τ^h simulations to maintain the grid spacing fixed. In LES, two computational grids were considered: a *coarse* grid made of $32 \times 32 \times 65$ nodes and a *fine* grid made of $64 \times 64 \times 65$ nodes. Only the lower value, Re_τ^l, of the shear Reynolds number was considered.

For the DNS, the number of grid points in each direction was chosen to ensure that the grid spacing is always smaller than the smallest flow scale[1] and the requirements imposed by the point-particle approach are satisfied. Assuming that particle motions due to strain are negligible, these requirements deal primarily with the size of the particle, which must be much smaller than the grid cell to justify the approximation that the velocity $\mathbf{u}_{@p}$ used in Eq. (7) is the (undisturbed) fluid velocity at the center of the particle. This velocity is obtained by interpolation and an accurate estimate requires a grid cell significantly larger than the particle. The accuracy of the fluid flow simulation, however, also requires a grid cell significantly smaller than the fluid scales to solve: if the particles are much smaller than the smallest relevant flow scale, than the point-particle restriction is satisfied. In the case of DNS, this means that particles must be much smaller than the Kolmogorov length scale ($d_p << \eta_K$). In one-way coupling simulations, violation of the above restrictions on particle size may introduce significant errors. For heavy particles in gas flows ($\rho_p/\rho \gg 1$), however, the time scale of the particles is significantly larger than the smallest fluid time scale: due to their inertia, the particles act as low-pass filters and are driven mostly by the large scales. The error introduced by a small grid cell is not important and may be neglected, the only consequence being that the particles experience a local flow field with smaller scales than the ones that are actually forcing the particles (Portela and Oliemans, 2003).

Samples of $n_p = 10^5$ particles characterized by different response times were considered for each value of the shear Reynolds number. The response time is made dimensionless using wall variables, and the Stokes number is thus obtained as $St \equiv \tau_p^+ = \tau_p/\tau_f$ where $\tau_f \equiv \nu/u_\tau^2$ is the viscous timescale of the flow. This characteristic time scale supplies a measure of the time available for eddy–particle interaction. Tables 1 and 2 summarize the complete set of parameters relevant to the simulations of particle dispersion, including the non-dimensional values of the stationary average settling velocity of the particles, V_s^+, and the corresponding values of the particle Reynolds number, Re_p. We remark that the characteristic timescale of the flow changes depending on the specific value of the shear Reynolds number, namely on the specific value of the shear velocity. In the present case, we have $\tau_f^l = \nu/(u_\tau^l)^2 = 1.13 \times 10^{-3}$ s for the Re_τ^l simulations and $\tau_f^h = \nu/(u_\tau^h)^2 = 2.83 \times 10^{-4}$ s for the Re_τ^h simulations. For the present channel flow configuration at Re_τ^l, the non-dimensional value of the Kolmogorov timescale, τ_K^+, ranges from 2 wall units at the wall to 13 wall units at the channel centerline (Marchioli et al., 2006). Hence, if we rescale the particle response times given in Table 1 using the local value of τ_K^+ near the centerline, where the flow conditions are closer to homogeneous and isotropic, we obtain Stokes numbers that vary from 10^{-2} to 10. In this paper, we will present results encompassing a total number of 17 cases (11 in DNS fields, 6 in LES fields), which represent a complete and homogeneous source of data covering a large target parameter space. A repository of both post-processed and raw data for the St^l particles was gathered in the frame of an international collaboration (see Marchioli et al., 2008c) and is available online at http://cfd.cineca.it. This *base* repository (including drag and inertia only) is complemented by other repositories including also the effects of gravity and lift in the same channel flow (see Marchioli et al., 2007).

[1] In the present flow configuration at Re_τ^l, the non-dimensional Kolmogorov length scale, η_K^+, varies along the wall-normal direction from a minimum value $\eta_K^+ = 1.6$ at the wall to a maximum value $\eta_K^+ = 3.6$ at the centerline. The grid resolution in the wall-normal direction is such that the first collocation point is at $z^+ = 0.05$ from the wall, while in the center of the channel $\Delta z^+ = 3.7$ (Marchioli et al., 2006).

3. Discussion

3.1. Phenomenology of particle deposition, entrainment and trapping phenomena

Particle transfer processes are dominated by the dynamics of turbulent structures in the proximity of the wall. As anticipated, we will review here some of the most relevant phenomena characterizing particle dynamics in the turbulent boundary layer. To explore the fundamental underlying physics, we will resort to concepts, ideas and models derived from direct numerical simulations of pointwise particle dispersion subject to inertia and drag in turbulent channel flow. We refer the reader to previous works (Brooke et al., 1992; Jimenez and Pinelli, 1999; Adrian et al., 2000; Marchioli and Soldati, 2002; Schoppa and Hussain, 2002; Soldati, 2005; Adrian, 2007) for details and in-depth explanations.

A pictorial view of particle transport mechanisms is provided in Fig. 2, where one instantaneous snapshot of particle distribution and turbulent coherent structures in the near-wall region of the channel is shown. Here, we focus on a cross-sectional window ($y - z$ plane) of the computational domain having thickness equal to one streamwise cell. Fig. 2(a) shows the flow field in a region of strong particle accumulation between two subsequent QSV. Vectors represent the fluid velocity in the plane and color isocontours map the values of the streamwise velocity component. A strongly coherent ejection of low-momentum fluid is apparent in the middle of the figure, where one low-speed streak is lifted and flanked by two counter-rotating QSV. In-sweeps of high-momentum fluid are also visible on the downwash side of the QSV. Particle position is identified with the circles – larger than the real scale for ease of visualization. Blue particles have wall-normal velocity directed away from the wall whereas purple particles have wall-normal velocity directed toward the wall. In Fig. 2(b) we show the same flow field but this time we focus on the flow structures, identified using streamwise vorticity isosurfaces. The green isosurface identifies the counter-clockwise rotating QSV, whereas the pale blue isosurface identifies the clockwise rotating QSV. Particle color code is the same as in Fig. 2(a).

The structures depicted in Fig. 2 control the deposition process: (i) they accumulate particles in a region not far from the wall; (ii) they produce the sweeps which bring particles to the wall; (iii) they may trap particles in the wall region or (iv) they may entrain particles again in the outer flow. It was shown previously that particles are either re-entrained immediately by the same vortex which brought them to the wall or confined for very long times in the viscous region (Narayanan et al., 2003). As a consequence, particle transfer fluxes toward the wall have higher intensity than particle transfer fluxes away from the wall. In turn, unbalanced fluxes lead to non-uniform (preferential) distribution of particles within the flow and produce near-wall particle accumulation (Reeks, 1983; Marchioli and Soldati, 2002).

3.2. Statistical description of particle trapping and resuspension mechanisms

As for particle deposition, the proper timing between particles and coherent structures is of fundamental importance for resus-

Please cite this article in press as: Soldati, A., Marchioli, C. Physics and modelling of turbulent particle deposition and entrainment: Review of a systematic study. Int. J. Multiphase Flow (2009), doi:10.1016/j.ijmultiphaseflow.2009.02.016

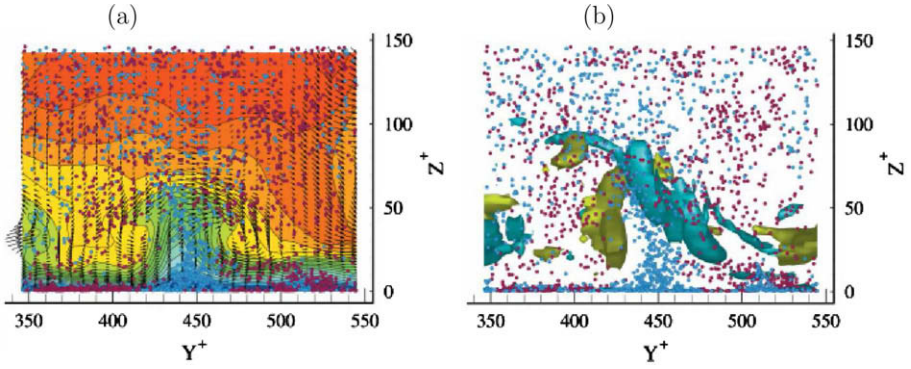

Fig. 2. Cross-section of the flow field and front view of particles in the region of particle accumulation (a) and front view of particles and structures in the region of particle accumulation (b).

pension, since particles can only leave the wall layer through fluid ejections. Particles driven to the wall by a sweep and not re-entrained to the outer flow by an ejection are bound to remain in the viscous wall layer for long times, slowly diffusing to the wall due to turbophoresis (Reeks, 1983; Narayanan et al., 2003). Clearly, the mechanism of particle re-entrainment from the viscous sublayer is influenced by inertia. QSV control particle resuspension via the ejections they generate. However, one can intuitively argue that larger particles will require larger momentum than smaller particles. To characterize the influence of inertia on particle resuspension it is thus important to establish a quantitative link between the inertia of the re-entrained particle and the *strength*, e.g. size and turnover time, of the structure responsible for re-entrainment. This type of analysis is also useful to understand exactly where resuspended particles come from, namely to understand whether particles have been just swept to the wall layer or have been sitting there for a long time.

Fig. 3(a) shows the probability density function (PDF) of the non-dimensional particle residence time, t^+_{res}, in the viscous sublayer – threshold fixed at $z^+ = 5$. Profiles for all the particle sets of Table 1 are shown. To compute t^+_{res} a time counter is started for each particle entering the viscous sublayer, the time counter is then stopped when the particle exits the viscous sublayer. A short residence time indicates that a particle penetrating the viscous sublayer may exit by being transported on the same vortical structure which brought it inside in the first place. All curves in Fig. 3(a) follow a similar trend for $t^+_{res} > 40$, so our analysis is focused on shorter residence times. Each curve has a rather well defined peak: the PDF reaches its maximum value at $t^+_{res} \simeq 7$ for the $St^l = 0.2$ and $St^l = 1$ particles; between 7 and 13 for the $St^l = 5$ particles; and about $t^+_{res} \simeq 20$ for the larger $St^l = 25$ and $St = 125^l$ particles. It is interesting to compare these peak values with the characteristic timescale of the turbulent structures in the near-wall region. This timescale, given here in terms of local dimensionless eddy turnover time, $t^+_{eddy} \equiv 1/\omega^+_x$ (where ω^+_x is the streamwise fluid vorticity), is shown in Fig. 3(b) as a function of the wall distance, z^+. Considering that t^+_{eddy} scales linearly with z^+ within the viscous sublayer and decreases progressively as the structures lie closer to the wall, we first observe that large particles may exit the viscous sublayer quickly *only if re-entrained* by large structures. Second, re-entrainment mechanisms for small particles are dominated by those structures with turnover time $t^+_{eddy} \simeq 7$ in wall units.

The transport mechanisms described so far are summarized in the schematics of Fig. 4. First, particles segregate and form coherent clusters in regions of the buffer layer where in-sweeps can entrain them: segregation into clusters is thus the first mechanism characterizing the deposition process. Particles entrained in a sweep experience a net drift toward the near-wall accumulation region, where particle concentration reaches its maximum. In the physical situation under investigation, the main mechanism capable of inducing such drift is turbophoresis (Narayanan et al., 2003; Marchioli et al., 2003). Once in the accumulation region, which is located well into the viscous sublayer, particles may either deposit at the wall or be re-entrained toward the outer flow by ejections. Two main deposition mechanisms can be identified (Portela et al., 2002; Narayanan et al., 2003): particles that have acquired enough momentum may coast through the accumulation region and deposit by impaction directly at the wall; otherwise, after a long residence time, particles can deposit under the action of turbulent fluctuations which are strictly zero only at the wall and, due to turbulence non-homogeneity, are always stronger in driving

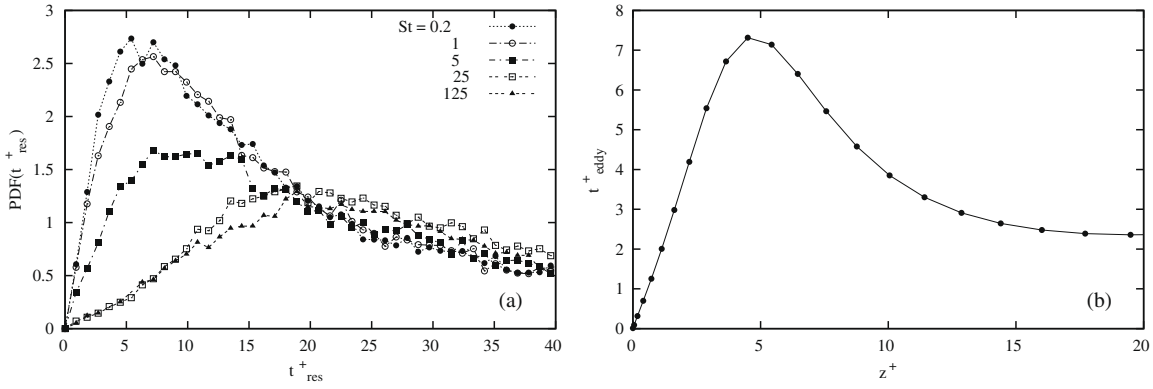

Fig. 3. PDF of the particle residence time, t^+_{res}, in the viscous sublayer (a); and local eddy turnover time, t^+_{eddy}, as a function of the wall-normal coordinate, z^+ (b).

Please cite this article in press as: Soldati, A., Marchioli, C. Physics and modelling of turbulent particle deposition and entrainment: Review of a systematic study. Int. J. Multiphase Flow (2009), doi:10.1016/j.ijmultiphaseflow.2009.02.016

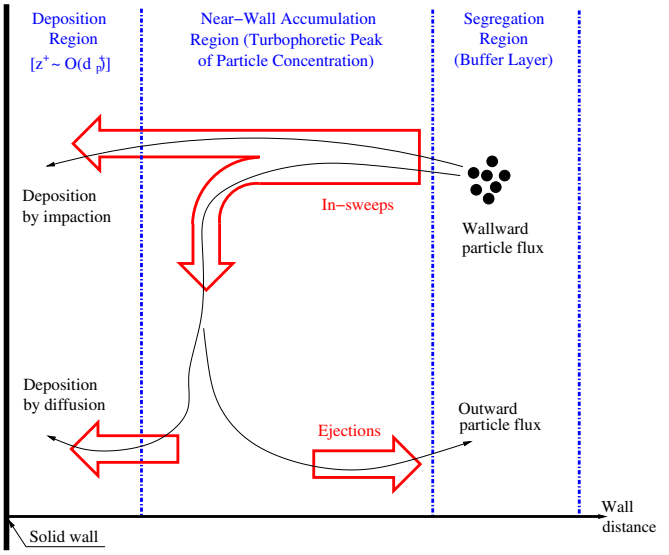

Fig. 4. Near-wall driving mechanisms, responsible for particle concentration build-up in the near-wall accumulation region.

particles to the wall. The relative importance of these two mechanisms depends on particle inertia.

3.3. Statistical description of particle preferential distribution, segregation and deposition

As discussed in the previous sections, particle deposition can be regarded as the outcome of a multi-step process: segregation → accumulation → deposition. In the following a number of statistical tools that can be used to characterize from a statistical viewpoint all these steps will be surveyed. Our analysis will restrict to the physical situation in which, while velocity statistics for both phases are at stationary state, particle distribution is still developing and much longer simulation times would be required to obtain steady-state concentration profiles (Marchioli et al., 2008c). The rationale for this choice is that, in a number of industrial applications including separation (Soldati and Banerjee, 1998; Soldati, 2000) and droplet-laden flows (Soldati and Andreussi, 1996), particle distribution never reaches equilibrium. From an engineering viewpoint, statistically-developing particle concentration is thus the most probable (and the most interesting) situation to investigate.

3.3.1. Quantification of particle preferential distribution in the viscous sublayer

In recent years, several studies (e.g. Picciotto et al., 2005; Rouson and Eaton, 2001; and references therein) were conducted to correlate particle distribution in the viscous sublayer with coherent structures based on global statistical identifiers. A methodology was thus developed to correlate non-homogeneous particle accumulation to coherent flow structures, according to their topological properties. A general flow topology classification was proposed (see Blackburn et al. (1996) for details) to group all elementary three-dimensional flow patterns with respect to the three invariants, P, Q and R, of the velocity gradient tensor, $u_{i,j}$. For incompressible flow fields:

$$P \equiv u_{i,i} = 0, \tag{8}$$

$$Q \equiv \frac{1}{2}\left[(u_{i,i})^2 - u_{i,j}u_{j,i}\right] = \frac{1}{2}(\Omega_{ij}\Omega_{ij} - S_{ij}S_{ij}), \tag{9}$$

$$R \equiv -\lambda_1\lambda_2\lambda_3, \tag{10}$$

and $D = (27/4)R^2 + Q^3$ is the discriminant that determines the eigenvalues λ_1, λ_2 and λ_3 of $u_{i,j}$. The quantities $\Omega_{ij} \equiv \frac{1}{2}(u_{i,j} - u_{j,i})$ and $S_{ij} \equiv \frac{1}{2}(u_{i,j} + u_{j,i})$ are the antisymmetric and symmetric components of the velocity gradient, respectively. Four regions can be identified across the curves $D = 0$ and $R = 0$: two vortical flow regions, the so-called stable focus/stretching (I) and unstable focus/compressing critical nodes (II), and two convergence regions, the so-called stable node/saddle/saddle (III) and unstable node/saddle/saddle critical nodes (IV). Further critical points can be identified along the Q-axis and the $D = 0$ line. The reader is referred to the papers by Cantwell and co-workers for a complete treatment (see Chacin and Cantwell (2000) or Blackburn et al. (1996), for instance).

The structural classification scheme employed by Blackburn et al. (1996) eliminates the arbitrary choice of threshold values required by other schemes and, therefore, it can be conveniently used to elucidate the relationship between particle distribution and near-wall vortices. In their DNS study, Rouson and Eaton (2001) focused their attention on moderate- to high-Stokes number particles ($St = 8.6$, 117, and 810) throughout the entire channel. This range includes particles too big to match the ever-decreasing turbulent flow scales which particles encounter when approaching the wall. In a subsequent DNS study (Picciotto et al., 2005), we tried to complement the analysis of Rouson and Eaton (2001) by considering low- to moderate-Stokes number particles, which are more "respondent" to the near-wall flow timescales. Since we are interested in providing a statistical description of particle preferential distribution very near the wall, in Fig. 5 we show the joint probability density function (JPDF) of Q and R in the viscous sublayer only. JPDFs were calculated over 400 realizations of the flow field (covering 1800 dimensionless time units) to consider only those events with significant statistical occurrence.

The JPDF sampled for the fluid at grid points (Fig. 5(a)) shows that the most probable value of Q and R is zero for all the instants, and that the preferred quadrants correspond to the stable focus/stretching (II) and the unstable node/saddle/saddle (IV) topologies. Also, the lines of constant JPDF asymptote toward the $D = 0$ curve, which represents the tail of the tear-drop shaped (Q, R)-distribution. As expected, the JPDF sampled at the position of the smaller particles ($St^l = 0.2$ in Fig. 5(b) and $St^l = 1$ in Fig. 5(c)) is similar to that of the fluid and shows weak preferential distribution. The degree of particle preferential sampling increases monotonically up to the intermediate-size particles: the area covered in the (Q, R)-plane by the JPDFs becomes smaller (see Fig. 5(d) and (e)), indicating that these particles avoid the strongest vortical regions in quadrants I and II as well as the strongest vortex-stretching regions (quadrant IV) along the positive-R, zero-D curve. Only convergence regions (III) are characterized by particle preferential sampling. A broader JPDF is obtained again for the $St^l = 125$ particles, as shown in Fig. 5(f). This demonstrates the effect of the Stokes number on particle preferential sampling. Results from percent particle counts for each topological quadrant and for each particle set (reported in Picciotto et al., 2005) corroborate the conclusion that a larger proportion (more than 70%) of particles tends to occupy convergence regions in the viscous sublayer, while the strongest vortical regions are depleted of particles due to the centrifuge-like effect of the eddies in the near-wall region (Rouson and Eaton, 2001).

Particles may remain long time or short time in the accumulation regions (Narayanan et al., 2003). Yet, the analysis in the (Q, R)-space may not discriminate between long- and short-term accumulation in convergence regions. A different identification criterion specifically valid in the wall proximity is thus required. One possibility is to exploit the relationship between the fluctuating components of the wall shear stress, τ'_{ij}, and the fluctuating components of the velocity gradient tensor evaluated at the wall, $u'_{i,j}|_w$. Limiting the analysis to incompressible flow, the only non-vanish-

Please cite this article in press as: Soldati, A., Marchioli, C. Physics and modelling of turbulent particle deposition and entrainment: Review of a systematic study. Int. J. Multiphase Flow (2009), doi:10.1016/j.ijmultiphaseflow.2009.02.016

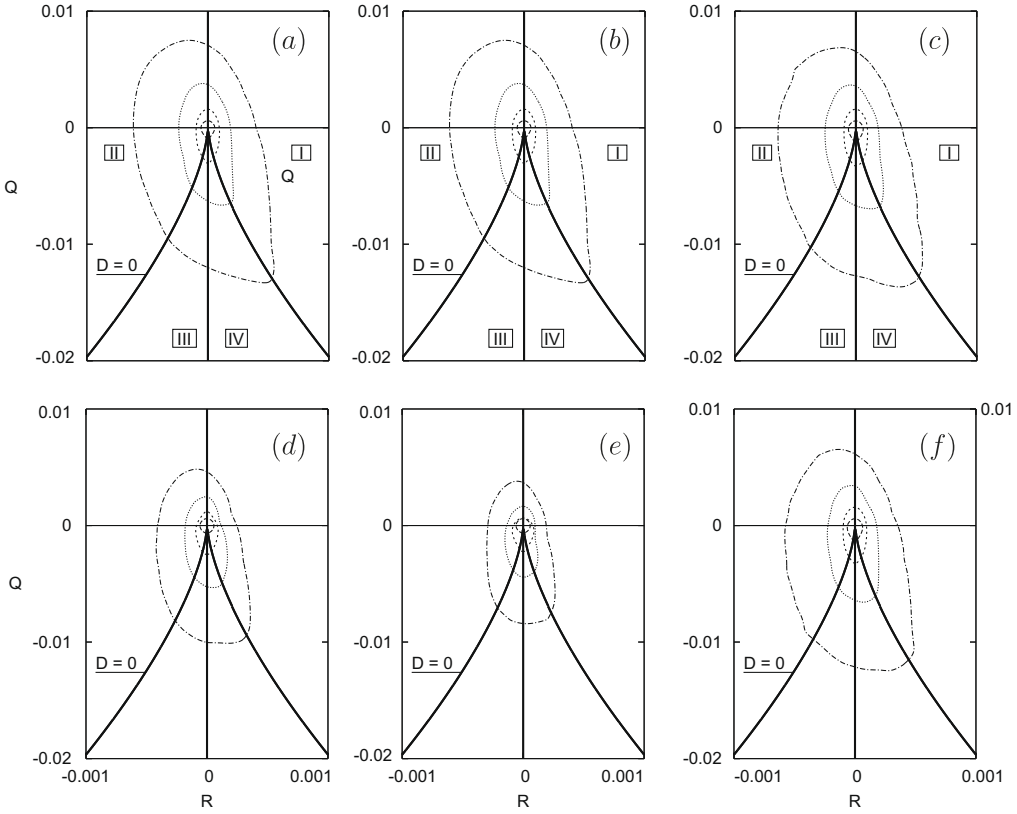

Fig. 5. Viscous sublayer ($z^+ < 5$) joint PDF of Q, R conditionally sampled for fluid at grid points (a) and at particle positions (b–f). (b) $St^I = 0.2$; (c) $St^I = 1$; (d) $St^I = 5$; (e) $St^I = 25$; (f) $St^I = 125$. Isoline values are: – – JPDF = 10, - - - JPDF = 1, ··· JPDF = 0.1, –·– JPDF = 0.01.

ing components of this tensor at the wall are $u'_{x,z}|_w = \partial u'/\partial z|_w$ and $u'_{y,z}|_w = \partial v'/\partial z|_w$. Now, the low-speed streaks are ejection-like environments that correlate with lower-than-mean wall shear stress regions ($\tau'_{xz}|_w \equiv \mu \cdot \partial u'/\partial z|_w < 0$), whereas the high-speed streaks are associated with higher-than-mean wall shear stress regions ($\tau'_{xz}|_w > 0$). More specifically, two distinct near-wall flow regions can be identified with respect to the wall-normal direction: a sweep-like inflow region, characterized by $\tau'_{yz}|_w \equiv \mu \cdot \partial v'/\partial z|_w = 0$ associated to $\tau'_{xz}|_w > 0$, and an ejection-like outflow region, characterized by $\tau'_{yz}|_w = 0$ associated to $\tau'_{xz}|_w < 0$.

Fig. 6 shows the instantaneous joint correlations of non-vanishing components of $u'_{i,j}|_w$. Correlations were computed for both the fluid and the particles following the same procedure as in Picciotto et al. (2005). Visual inspection indicates that, regardless of particle size, particles in the viscous sublayer accumulate preferentially in the negative $\partial u'/\partial z|_w$ semiplane, which corresponds to ejection-like low-speed regions near the wall. This is also confirmed by the percentage of sample points falling in each $\partial u'/\partial z|_w$ semiplane (percent figures are included in Fig. 6). Note that even the fluid (Fig. 6(a)) shows preferential distribution: a clear consequence of the mechanism by which fluid velocity streaks are generated. A jet of fluid directed to the wall generates the sweep and also the high-speed region; then the jet of fluid, by continuity, is deflected by the wall and generates the ejection. Due to the entrainment of surrounding fluid, the sweep is more intense and concentrated while the ejection spreads over a wider cross-section and has lower momentum. Low-speed, low-shear regions, where $\tau'_w < 0$ (i.e. $\partial u'/\partial z^+|_w < 0$), appear much wider than high-speed, high-shear regions, where $\tau'_w > 0$ (i.e. $\partial u'/\partial z^+|_w > 0$). Thus, grid points necessarily sample $\partial u'/\partial z^+|_w < 0$ regions more often. The correlations shown in Fig. 6 are similar for all the flow field realizations we studied (the same that were used to obtain Fig. 5). Percent data for samples falling in each $\partial v'/\partial z|_w$ semiplane (not shown) also indicate that the preferred near-wall flow regions correlate well with values of $\partial v'/\partial z|_w$ close to zero, thus leading to the conclusion that particle concentration build-up occurs preferentially in the proximity of a near-wall outflow region (Picciotto et al., 2005).

The physics described in Fig. 6 can be examined also in Fig. 7. This figure shows the instantaneous distribution of the $St^I = 25$ particles, chosen for their relatively larger tendency to preferential sampling (see discussion of Fig. 5), together with the contours of $\tau'_{xz}|_w$ in the (x, y)-plane. The behavior of $\partial u'/\partial z^+|_w$ along the spanwise direction at a fixed streamwise location (identified with the dash-dotted *AA*-line) is also shown on top of Fig. 7. Dark gray spheres represent particles with positive spanwise velocity ($v > 0$), moving from left to right; light gray spheres represent particles with negative spanwise velocity ($v < 0$), moving from right to left. Dark gray contours indicate high positive values of $\tau'_{xz}|_w$, white contours indicate low negative values. Black solid lines connect points where $\tau'_{yz}|_w$ is equal to zero. From Fig. 7, it is apparent that particles arriving at the wall are initially found in high-speed, high-shear regions (white contours), which are convergence flow regions where $\partial u'/\partial z|_w$ attains a local maximum. Particles stay briefly in the high-speed regions: they are swept away from these regions and clusters begin to split along the $\partial v'/\partial z|_w = 0$ lines, which thus mark the position of Short-Term Accumulation (*STA*) regions. Particles move in the spanwise direction toward low-speed, low-shear regions (dark gray contours), where $\partial u'/\partial z|_w$ attains a local minimum – i.e. the low-speed streaks. In these regions, particles line up and form persistent clusters flanking the $\partial v'/\partial z|_w = 0$ lines, which now mark the position of Long-Term Accumulation (*LTA*) regions.

3.3.2. Quantification of particle segregation

In the previous sections, we have discussed some statistical tools that can provide a quantitative description of near-wall phe-

Please cite this article in press as: Soldati, A., Marchioli, C. Physics and modelling of turbulent particle deposition and entrainment: Review of a systematic study. Int. J. Multiphase Flow (2009), doi:10.1016/j.ijmultiphaseflow.2009.02.016

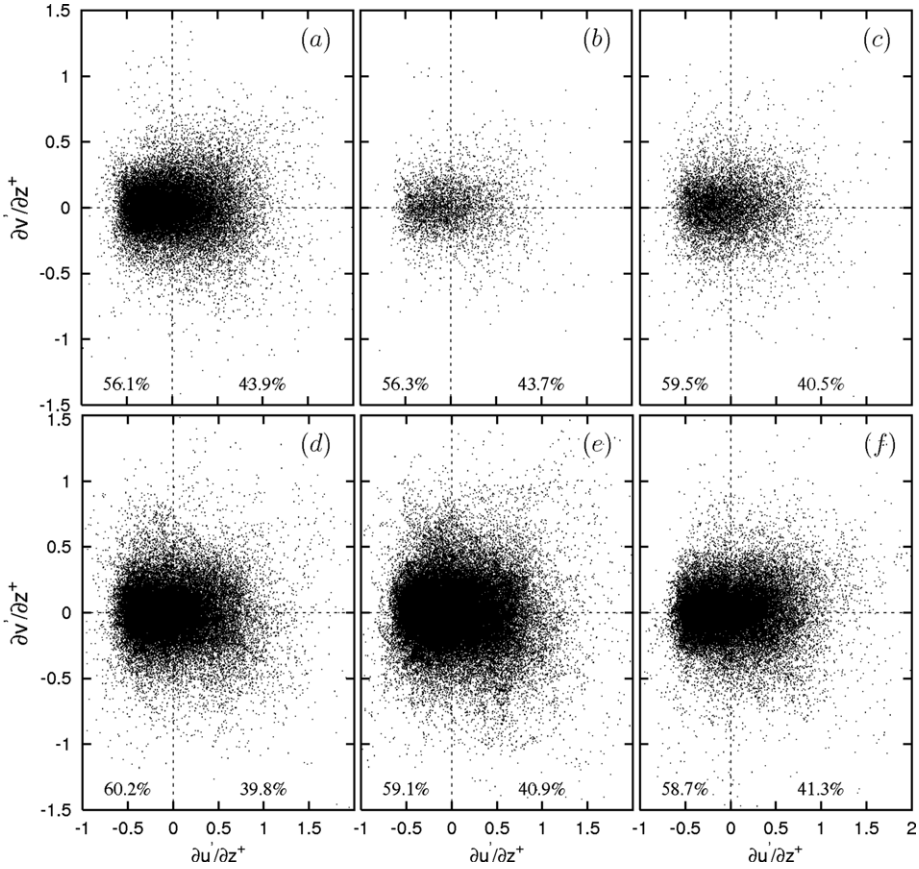

Fig. 6. Viscous sublayer ($z^+ < 5$) instantaneous joint correlations of non-vanishing components of the fluctuating velocity gradient tensor, conditionally sampled at the fluid grid points (a) and at particle positions projected onto the wall (b–f). (b) $St^I = 0.2$, (c) $St^I = 1$, (d) $St^I = 5$, (e) $St^I = 25$, (f) $St^I = 125$. Joint correlations demonstrate that particles are mostly concentrated in the ejection-like environments. Percent figures indicate the number of particles in a region of positive/negative $\partial u'/\partial z|_w$.

nomena such as particle trapping/re-entrainment (Section 3.2) and particle preferential distribution (Section 3.3.1). In the following, we will present additional statistical tools that can be used to characterize particle segregation and particle deposition. These tools have been used also to characterize and optimize particle dispersion in jets (Campolo et al., 2008; Sbrizzai et al., 2009, 2004; Campolo et al., 2005).

The relative tendency of particles to segregate in a turbulent flow field can be quantified in terms of maximum deviation from randomness, D (Fessler et al., 1994), also referred to as segregation parameter, Σ_p (Février et al., 2005). The maximum deviation from randomness is defined as:

$$D \equiv \frac{\sigma - \sigma_{\text{Poisson}}}{\mu}, \tag{11}$$

where σ is the standard deviation for the measured particle number density distribution and σ_{Poisson} is the standard deviation for a Poisson distribution (i.e. a purely random distribution of the same average number of particles). The parameter μ is the mean particle number density. According to Eq. (11), $D = 0$ corresponds to a random distribution, $D < 0$ corresponds to a uniform distribution, and $D > 0$ indicates segregation of particles. In this latter case, larger values of D correspond to stronger segregation. The maximum deviation from randomness was applied to homogeneous isotropic turbulence (Février et al., 2005) and to the centerline of a turbulent channel flow (Fessler et al., 1994), focusing on two-dimensional regions of nearly homogeneous flow to observe particle response to small scale turbulent motions. In our channel flow simulations, the use of D was extended to the near-wall region, where inhomogeneities arise in the direction perpendicular to the wall. The particle number density distribution is thus computed on a three-dimensional grid containing N_{cell} cells of volume Ω_{cell} covering the entire computational domain. This grid is independent of the Eulerian grid used by the flow solvers, and the volume Ω_{cell} is varied by changing the streamwise and the spanwise lengths of the cell whereas the wall-normal length is maintained to a uniform size to avoid an additional averaging scale in the wall-normal direction. The value calculated for D depends on the cell size. Because of this dependency, the segregation parameter can not provide an absolute, clearcut quantification of particle segregation; rather it should be used just to identify and compare different trends. Taking this into account, the cell size dependency can be partially overcome by computing the particle number density distribution for several values of Ω_{cell} and keeping only the largest value of D (Sbrizzai et al., 2009; Picciotto et al., 2005; Février et al., 2005). This choice is justified by the following reason: the cell size for which D is maximum indicates the length scales of particles clustering.

Fig. 8 shows the maximum deviation from randomness, D_{max} (black circles), as a function of the particle Stokes number, St^I, in the viscous sublayer ($0 < z^+ < 5$). Values indicate that the maximum segregation is obtained for the $St^I = 25$ particles, which also exhibit the strongest tendency to sample preferentially the flow field (see Fig. 5). This indicates that particle dynamics in the viscous sublayer is controlled by flow structures with non-dimensional timescale $\tau_f^+ \simeq 25$. Considering that τ_f^+ scales linearly with wall distance and decreases progressively as the turbulence structures lie closer to the wall, we can infer that this value corresponds to the circulation time of the turbulence structures in the buffer layer ($5 < z^+ < 30$).

It is helpful to complement the analysis on particle segregation by providing a single quantitative measure rather than the two numbers, D and the length scale for that value of D. Several possi-

Please cite this article in press as: Soldati, A., Marchioli, C. Physics and modelling of turbulent particle deposition and entrainment: Review of a systematic study. Int. J. Multiphase Flow (2009), doi:10.1016/j.ijmultiphaseflow.2009.02.016

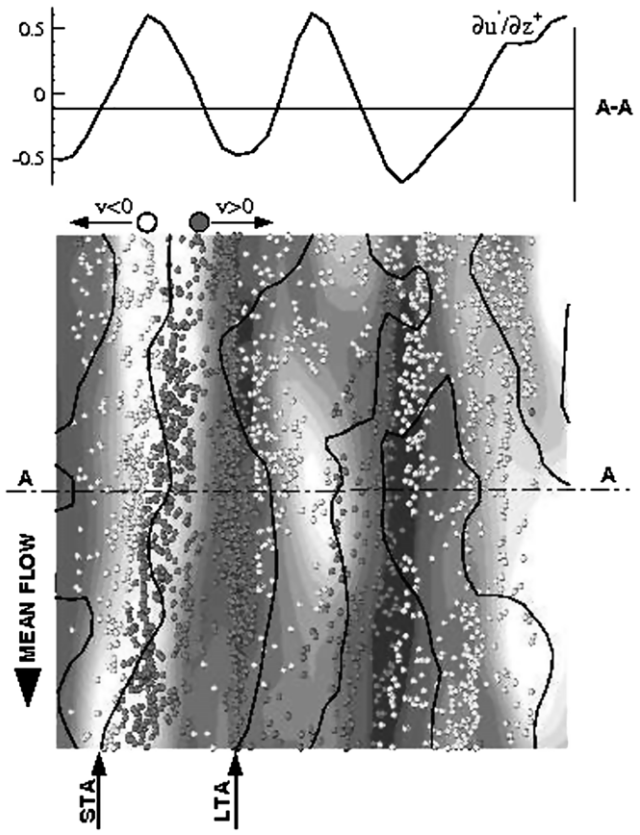

Fig. 7. Instantaneous $St^l = 25$ particle distribution in the viscous sublayer ($t^+ = 6500$, $z^+ < 5$). The computational window is 400 wall units long and 250 wall units wide in the (x, y)-plane. The mean flow is directed top down.

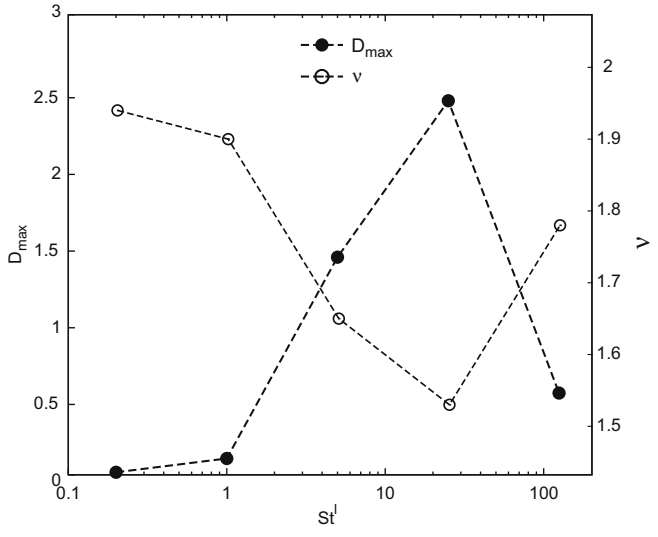

Fig. 8. Maximum deviation from randomness, D_{max} (black circles), and correlation dimension, v (open circles), in the viscous sublayer as a function of the particle Stokes number, St^l. Data are relative to the no-gravity, no-lift case. Values of D_{max} are instantaneous (computed at $t^+ = 6500$, corresponding to the final instant in the computation of the statistics shown in Figs. 5 and 6). Values of v are time-averaged (over $t^+ = 1800$ time units).

bilities to measure segregation have been identified (see, for instance, Calzavarini et al., 2008). Here, we will compute the correlation dimension, introduced by Grassberger and Procaccia (1983). In its three-dimensional formulation, needed to study non-isotropic flows, this parameter can be computed by choosing one base particle and counting the fraction, $N_p(r)$, of particles within a distance r from the base particle. The correlation dimension, v, is defined as the slope of $N_p(r)$ as a function of r in a log–log plot. The probability distribution of the distance between the neighboring particles and the base particle is obtained repeating this count for all possible values of r, thus removing any dependence on the length scale used. In general, $N_p(r)$ will scale with r^v: if particles are uniformly distributed in the volume surrounding the base particle, $N_p(r)$ will scale with r^3 (namely with the volume of the sphere centered on the base particle); if particles are uniformly distributed over a surface, $N_p(r)$ will scale with r^2 (namely with the area of the circle centered on the base particle), whereas if particles are concentrated into a line, $N_p(r)$ will scale with linearly with r. Thus smaller values of v indicate greater preferential concentration. To compute results significant from a statistical perspective, the procedure can be repeated for different randomly chosen base particles and different times, averaging the results. The correlation dimension calculated for the particles in the base DNS at Re_τ^l is shown in Fig. 8 (open circles). The correlation dimension is always smaller than 2, indicating that, regardless of their size, particles never attain a uniform spatial distribution. It is confirmed that, while nearly random distribution is observed for the smaller particles, preferential concentration is maximum for particles with Stokes numbers around 25. In particular, the minimum value $v \simeq 1.53$ indicates that the preferential accumulation of these particles mainly occurs in elongated structures.

3.3.3. Influence of the Reynolds number on particle segregation

The results shown in Fig. 8 are relative to the case of turbulent channel flow at moderate Reynolds number (Re_τ^l). If higher values of Re_τ are to be considered, then Reynolds number effects on particle dispersion may become significant because the characteristic length and time scales of the particle change with respect to those of the fluid when the flow dynamics change: in particular, the higher the Reynolds number the smaller the particle response time for a given value of the Stokes number. This point can be further elucidated considering Fig. 9, where the one-dimensional (streamwise) frequency spectrum, $E(\omega)$, computed for the DNS at Re_τ^l is compared with the frequency spectrum computed for the DNS at Re_τ^h at the $z^+ = 25$ location inside the buffer layer. Also shown (solid vertical lines) are the estimated response frequencies, proportional to $1/\tau_p$, for each particle size. It is apparent that, in the Re_τ^h flow (i) the turbulent kinetic energy budget spreads over a wider range of frequencies, representing smaller flow timescales with

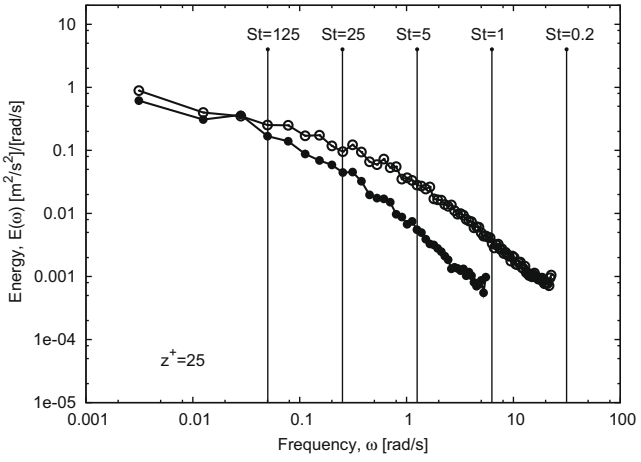

Fig. 9. One-dimensional (streamwise) frequency spectrum for turbulent channel flow computed at $z^+ = 25$ for two different Reynolds numbers: Re_τ^l (•) and Re_τ^h (○).

Please cite this article in press as: Soldati, A., Marchioli, C. Physics and modelling of turbulent particle deposition and entrainment: Review of a systematic study. Int. J. Multiphase Flow (2009), doi:10.1016/j.ijmultiphaseflow.2009.02.016

which the particles may interact, and (*ii*) a given value of frequency corresponds to higher values of the turbulent kinetic energy. In principle, these observations should lead to the conclusion that simulation techniques like LES, requiring models for the filtered subgrid fluid scales, must incorporate a dependency on the flow Reynolds number to recover the correct amount of SGS turbulent kinetic energy. In fact, the need to include Reynolds number effects should be carefully assessed being based on the knowledge of how particle preferential concentration scales with this parameter. Numerical investigations of the scaling properties of particle preferential concentration with the Reynolds number were performed in a synthetic turbulent advecting field by Olla (2002) and in Homogeneous Isotropic Turbulence (HIT) by Collins and Keswani (2004) and by Yeung et al. (2006).

Here, we investigate on the same effect in turbulent channel flow.

To introduce our scaling argument, we remark that the same (dimensional) value of the particle response time corresponds to different values of the Stokes number according to the following expression:

$$\tau_p^h = \tau_p^l \rightarrow St^h \cdot \tau_f^h = St^l \cdot \tau_f^l \rightarrow \frac{St^h}{St^l} = \frac{\tau_f^l}{\tau_f^h} = \left(\frac{u_\tau^h}{u_\tau^l}\right)^2 = \left(\frac{Re_\tau^h}{Re_\tau^l}\right)^2, \qquad (12)$$

where St^h and St^l represent the particle Stokes number in the Re_τ^h simulation and in the Re_τ^l simulation, respectively; and $(Re_\tau^h/Re_\tau^l)^2 = 4$ in our case. If the shear velocity is the proper scaling parameter then the coupling between particles and fluid in the regime where particles preferentially concentrate is expected to obey to Eq. (12). In Fig. 10 particle segregation in the center of the channel (Fig. 10(a)) and in the near-wall region (Fig. 10(b)) is quantified by the D_{max} parameter for the two DNS simulations. Black symbols represent the values of D_{max} for the particles in the DNS fields at Re_τ^l, whereas open symbols are used for the particles in the DNS fields at Re_τ^h. Two observations can be made: first, lower segregation occurs at higher Reynolds number for a given value of the particle Stokes number; second, the degree of segregation is indeed nearly the same for particle Stokes numbers and shear Reynolds numbers matching the condition given in Eq. (12), as indicated by the arrows. This is particularly true in the near-wall region. The above results seem to indicate that particle preferential concentration scales proportionally to the flow Reynolds number and that it is possible to parameterize Reynolds number effects simply by imposing a quadratic dependence of the particle Stokes number on the shear Reynolds number. These scaling effects appear to be consistent with other observations, most of which refer to the Kolmogorov scaling argument (Collins and Keswani, 2004; Yeung et al., 2006), that predict statistical saturation only at Reynolds numbers higher than those considered here.

3.3.4. Quantification of particle deposition rates

According to our schematism of the deposition process, the degree of particle segregation influences quantitatively the rate at which particles deposit (i.e. their deposition flux). This was explained in the previous sections considering the *chain* of physical mechanisms by which particles are transferred to and away from the wall. It is thus consequential to combine the quantitative description of particle segregation to the quantitative prediction of particle deposition rate. Virtually all the experimental data on the deposition rate were obtained in turbulent pipe flow. However, because deposition is mainly controlled by the near-wall turbulence, which is a local wall-dominated phenomenon not influenced by the largest scales of the flow, calculations for channel flow are the simplest setting for model validation. The deposition rate of non-interacting particles is proportional to the ratio between the particle mass transfer rate on the wall (flux of particles per unit deposition area), J, and the mean bulk concentration of particles (mass of particles per unit volume), C. According to this definition the constant of proportionality, named deposition coefficient $k_d \equiv -J/C$, represents a deposition velocity (Young and Leeming, 1997). Fig. 11 shows the non-dimensional values of the deposition coefficient, k_d^+, computed as function of the Stokes number in the Re_τ^l simulation (Picciotto et al., 2005). The trend is similar to that seen in Fig. 8, which refers to the same simulation time span: Again, the $St^l = 25$ particles exhibit the highest deposition rate. From our previous discussion, it is now easy to argue that this happens because these particles are the most responsive to near-wall turbulence in terms of segregation and preferential distribution. Particles with smaller or larger inertia are not able to respond in this *optimal* way, either because they behave more like tracers with strong stability against non-homogeneous distribution and near-wall concentration (the $St^l = 0.2$ particles, in particular), or because they are too big to respond optimally to the fine turbulence structures in the buffer layer (the $St^l = 125$ particles, for instance). In general terms, the degree of particle responsiveness to segregation and preferential distribution induced by the flow structures is strongly (and directly) correlated to the rate at which particles deposit.

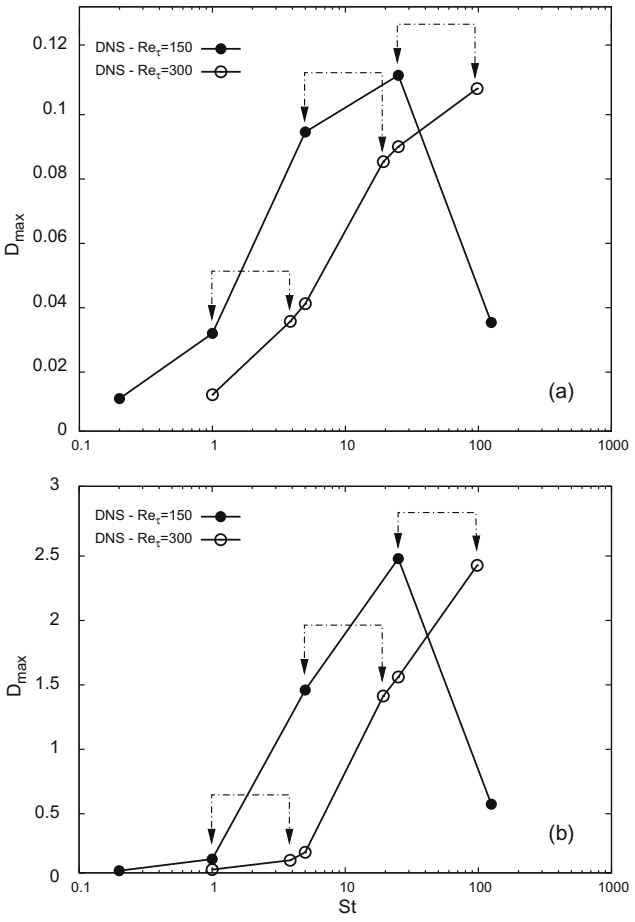

Fig. 10. Maximum deviation from randomness, D_{max}, versus particle Stokes number, St, in turbulent channel flow at two different Reynolds numbers: Re_τ^l (•) and Re_τ^h (○). Panels: (a) channel centerline ($145 \leqslant z^+ \leqslant 150$), (b) near-wall region ($0 \leqslant z^+ \leqslant 5$).

4. Modelling perspectives for Large-Eddy Simulation of turbulent dispersed flows

In this section, we will try to answer the issue of the minimal physics required to model particle motion at the subgrid level. This

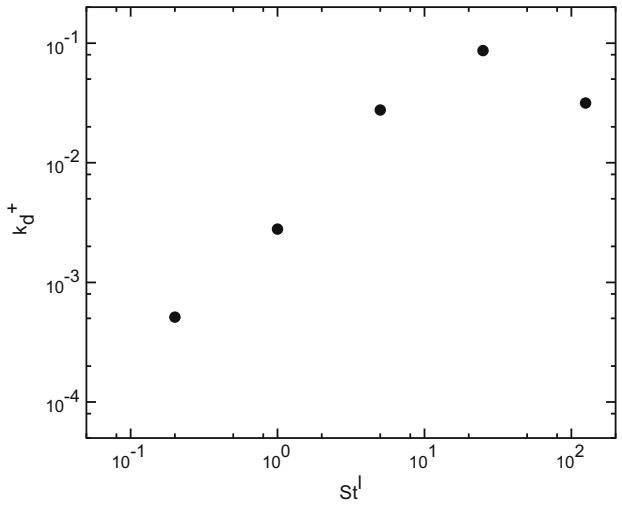

Fig. 11. Particle deposition coefficients, k_d^+, as a function of the particle Stokes number, St^l. Data are relative to the base no-gravity, no-lift simulation and are time-averaged from $t^+ = 4700$ to $t^+ = 6500$.

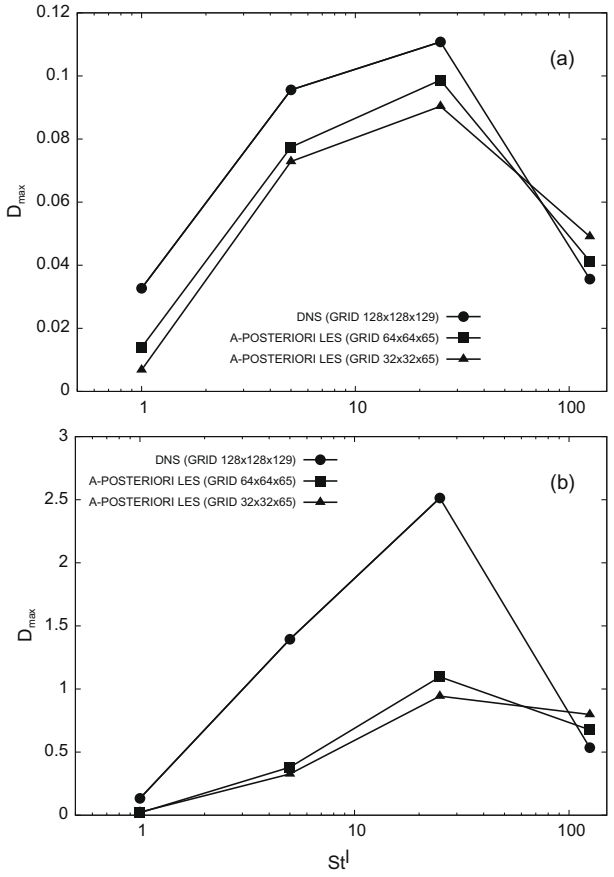

Fig. 12. Maximum deviation from randomness, D_{max}, versus particle Stokes number, St^l: comparison between DNS (○), *a-posteriori* LES on the fine $64 \times 64 \times 65$ grid (□) and *a-posteriori* LES on the coarse $32 \times 32 \times 65$ grid (△). Panels: (a) channel centerline ($145 \leqslant z^+ \leqslant 150$), (b) near-wall region ($0 \leqslant z^+ \leqslant 5$).

level is not solved by LES, preventing tracked particles from being exposed to flow scales which may influence their motion. Specifically, we will try to answer in a quantitative way to the following questions: How does the SGS turbulence affect particle dispersion? How should one model these SGS effects to predict accurately the selective response of different-inertia particles? Having in mind the phenomenological model illustrated in Section 3, we address these issues by analyzing first the effect of the subgrid fluid turbulence on particle segregation. Fig. 12 compares the DNS results for D_{max} against those obtained from *real a-posteriori* LES (Marchioli et al., 2008a). Here, we have adapted to our channel flow at Re_τ^l the computational procedure used by Fede and Simonin (2006) for the case of heavy colliding particles in HIT. LES fields were computed as discussed in Section 2. Particle tracking was performed with no extra model. In this way, the scales not resolved by LES are simply non-existing for the particle dynamics and it is possible to judge if some of the filtered scales effects should be included as suggested previously (Fede and Simonin, 2006; Kuerten, 2006). Results shown in Fig. 12 indicate that particle segregation is significantly influenced by the subgrid fluid turbulence, even when the particle response time is much larger than the flow timescales not resolved in LES. Both in DNS and in LES, the behavior of the segregation parameter is qualitatively similar: a peak of D_{max} occurs around $St^l = 25$ and preferential concentration falls off on either side of this *optimum* value. However, due to filtering, segregation is always underestimated by LES, except for the $St^l = 125$ particles. For these particles filtering leads to an increase of segregation, in agreement with the behavior observed by Fede and Simonin (2006). As expected, the quantitative inaccuracy of LES is particularly evident in the near-wall region (Fig. 12(b)), where the degree of misprediction depends strongly on the ratio of the particle size to the filtered spatial scales.

The limits of LES in providing an accurate quantitative estimate of local particle segregation have an effect on particle deposition fluxes and, in turn, on particle near-wall accumulation. This can be observed in Fig. 13, where different instantaneous particle concentration profiles (taken at time $t^+ = 1350$ of the simulations at Re_τ^l) are compared. Concentration is computed as particle number density distribution, C, normalized by its initial value, C_0 (see Marchioli et al. (2008a) for details). Only the intermediate-size particles are considered. For these particles, LES underpredicts both qualitatively and quantitatively particle accumulation at the wall. Compared to the DNS results, different-shape profiles and lower peaks of particle concentration inside the viscous sublayer are found. Note that the degree of underprediction also depends on the spatial resolution of the Eulerian grid. These findings are in line with previous LES applications to particle dispersion in turbulent wall-bounded flows (Kuerten and Vreman, 2005; Kuerten, 2006). In our opinion, Figs. 12 and 13 are important since they demonstrate that the inaccuracy of LES in predicting near-wall accumulation is a direct consequence of filtering, which removes both energy and flow structures from the LES turbulent flow field. LES may thus produce an inaccurate rendering of the near-wall vortices responsible for trapping particles in the viscous sublayer (Kuerten and Vreman, 2005). When these structures are smeared out of the flow field, their interactions with particles can not be fully captured and representation of local segregation phenomena becomes inadequate, in turn influencing macroscale collective phenomena as deposition and overall particle distribution (Marchioli et al., 2008a).

In the light of the above considerations, challenges for multiphase LES are in the specific modalities by which the SGS effects are recovered and incorporated into models. In recent years, several numerical studies have tried to clarify these modalities. Some authors (Kuerten and Vreman, 2005; Shotorban and Mashayek, 2005; Kuerten, 2006; Shotorban et al., 2007; Marchioli et al., 2008b) proposed a closure model for the equations of particle motion, which uses the approximate deconvolution method (Stolz et al., 2001) to reconstruct the filtered fluid velocity and add its effects in the particle equations. This model was assessed in different

Please cite this article in press as: Soldati, A., Marchioli, C. Physics and modelling of turbulent particle deposition and entrainment: Review of a systematic study. Int. J. Multiphase Flow (2009), doi:10.1016/j.ijmultiphaseflow.2009.02.016

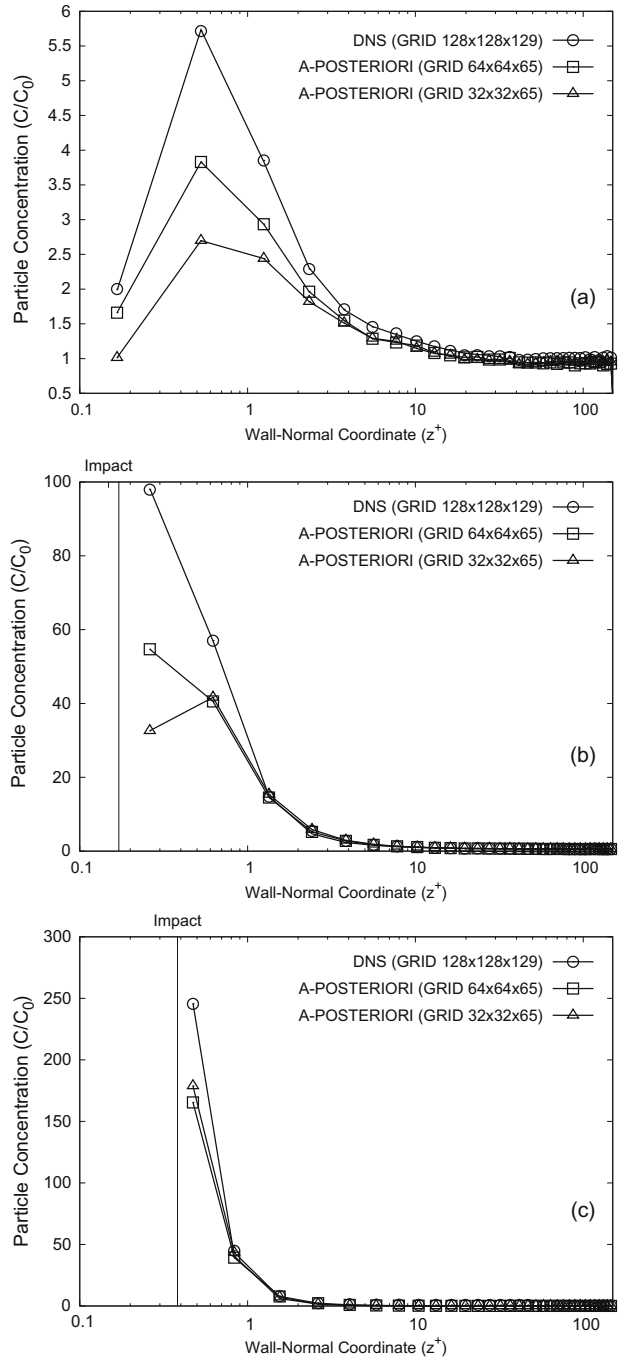

Fig. 13. Particle concentration in *a-posteriori* LES without SGS modelling in the particle equation of motion: comparison between DNS (○), *a-posteriori* LES on the fine $64 \times 64 \times 65$ grid (□) and *a-posteriori* LES on the coarse $32 \times 32 \times 65$ grid (△). Panels: (a) $St^I = 1$ particles, (b) $St^I = 5$ particles, (c) $St^I = 25$ particles. The vertical solid line in each diagram indicates the position where the particles hit the wall (*impact*): note that impact for the $St = 1$ particles occurs at $z^+ = 0.034$, outside the z^+-range covered in panel (a).

flow configurations (from homogeneous turbulent isotropic and shear flows to channel flow) and a general improvement in the prediction of particle-related statistics was observed. Obviously, deconvolution can be used to model the effect of the resolved scales only and subgrid scales, virtually non-existing in the LES context, can not be retrieved. These scales, however, do influence the instantaneous particle behavior (Kuerten, 2006). Hence, even when *ad hoc* closures are used in the particle equations, there might be situations in which prediction of local particle segregation and, in turn, of near-wall accumulation are judged inaccurate from a quantitative viewpoint because a quantitative *replica* of the subgrid turbulent flow scales is not ensured (Marchioli et al., 2008a). In our view, a model for subgrid particle dynamics may not be obtained by the information provided via a LES computation, rather it must be obtained via an independent physical reasoning. A modelling strategy that goes along this direction was developed recently by Minier and co-workers (Guingo and Minier, 2008; Chibbaro and Minier, 2008), who propose a Lagrangian model for particle deposition based on a stochastic description of the effects due to near-wall coherent structures. The idea behind this model is to account explicitly for the interactions of particles with the coherent sweep/ejection events by including the relevant geometrical features of the near-wall region. From an engineering viewpoint, this seems to be a very interesting and promising attempt to supply the particle equations with an adequate rendering of the flow field by capturing the relevant physics involved in the particle deposition process.

5. Conclusions

In this paper, we have reviewed the physical mechanisms responsible for deposition and entrainment of inertial particles in turbulent dispersed flow and have provided modelling perspectives for the numerical simulation of such processes. Interpretative models for the deposition and entrainment mechanisms were proposed and discussed on the basis of direct numerical simulations of turbulence and Lagrangian tracking of inertial particles. Simulations were performed adopting the pointwise particle approach and assuming that the interaction between the particle and the surrounding fluid is represented through a force located at the position of the particle center. This keeps the level of modelling to a minimum, provided that the inter-particle distance is large and particles are small compared with the smallest relevant flow scales. Even if the point-particle approach introduces some limitations to the modelling capabilities of the numerical methodology, and even if particle modelling is the simplest possible, simulations provide a fully representative three-dimensional and time-dependent description of the phenomena under investigation in the limit of *small* particles and dilute flow conditions.

Through the systematic application of this numerical methodology to a well-known archetypal instance of wall-bounded flow (particle-laden channel flow), we have provided a detailed view of the particle transfer mechanisms in turbulent boundary layer. From this perspective, the role of the near-wall coherent structures on each space and time scale involved, as well as the dispersion of particles characterized by different values of the inertia parameter has been considered carefully. In particular, we have pinpointed that particle deposition to a wall is quintessentially linked to particle accumulation into specific regions in the buffer layer. These findings are of particular importance for the improvement of existing deposition models and for the implementation of simulation techniques of broader engineering significance, such as LES. Results indicate that, since LES prediction of local segregation is inaccurate, also inevitably inaccurate will be the macroscale prediction of particle deposition and overall distribution. Thus, current capabilities of LES in Eulerian–Lagrangian studies of dispersed flows are strongly limited by the modelling of the subgrid scale turbulence effects on particle dynamics. These effects should be taken into account in order to reproduce accurately the physics of particle dispersion since the LES cut-off filter removes not only energy but, most important, flow structures from the turbulent flow field. This observation leads to the conclusion that recovering the subgrid energy by reconstruction of the correct amount of fluid and particle velocity fluctuations is not enough to reproduce the effect of SGS turbulence on particle near-wall accumulation.

Please cite this article in press as: Soldati, A., Marchioli, C. Physics and modelling of turbulent particle deposition and entrainment: Review of a systematic study. Int. J. Multiphase Flow (2009), doi:10.1016/j.ijmultiphaseflow.2009.02.016

Acknowledgements

The work presented in this paper has required a vast amount of support of all kinds. In particular, we are grateful to the following institutions for funding over the years: the Italian Ministry of Research (under PRIN and FIRB programs), the Italian Ministry of Productive Activities, and the Regional Authority of Friuli Venezia Giulia. C.M. also thanks the University of Udine for financial support. CINECA supercomputing center (Bologna, Italy) and HPC Europa Transnational Access Program are also gratefully acknowledged for generous allowance of computer resources.

References

Adrian, R.J., 2007. Hairpin vortex organization in wall turbulence. Phys. Fluids 19, 041301.

Adrian, R.J., Meinhart, C.D., Tomkins, C.D., 2000. Vortex organization in the outer region of the turbulent boundary layer. J. Fluid Mech. 422, 1–54.

Arcen, B., Tanière, A., Oesterlé, B., 2006. On the influence of near wall forces in particle-laden channel flows. Int. J. Multiphase Flow 32, 1326–1339.

Blackburn, H.M., Mansour, N.N., Cantwell, B.J., 1996. Topology of fine-scale motions in turbulent channel flow. J. Fluid Mech. 310, 269–292.

Brooke, J.W., Kontomaris, K., Hanratty, T.J., McLaughlin, J.B., 1992. Turbulent deposition and trapping of aerosols at a wall. Phys. Fluids A 4, 825–834.

Calzavarini, E., Kerscher, M., Lohse, D., Toschi, F., 2008. Dimensionality and morphology of particle and bubble clusters in turbulent flow. J. Fluid Mech. 607, 13–24.

Caporaloni, M., Tampieri, F., Trombetti, F., Vittori, O., 1975. Transfer of particles in nonisotropic air turbulence. J. Atmos. Sci. 32, 565–568.

Campolo, M., Cremese, A., Soldati, A., 2008. Controlling particle dispersion in a transverse jet by synchronized injection. AIChE J. 54, 1975–1986.

Campolo, M., Salvetti, M.V., Soldati, A., 2005. Mechanisms for microparticle dispersion in a jet in crossflow. AIChE J. 51, 28–43.

Cerbelli, S., Giusti, A., Soldati, A., 2001. ADE approach to predicting particle dispersion in wall bounded turbulent flows. Int. J. Multiphase Flow 27, 1861–1879.

Chacin, J.M., Cantwell, B.J., 2000. Dynamics of a low Reynolds number turbulent boundary layer. J. Fluid Mech. 404, 87–115.

Chibbaro, S., Minier, J.P., 2008. Langevin PDF simulation of particle deposition in a turbulent pipe flow. J. Aerosol Sci. 39, 555–571.

Cleaver, J.W., Yates, B., 1975. A sub layer model for the deposition of particles from a turbulent flow. Chem. Eng. Sci. 30, 983–992.

Collins, L.R., Keswani, A., 2004. Reynolds number scaling of particle clustering in turbulent aerosols. New J. Phys. 6, 1–19.

Fede, P., Simonin, O., 2006. Numerical study of the subgrid fluid turbulence effects on the statistics of heavy colliding particles. Phys. Fluids 18, 045103.

Fessler, J.R., Kulick, J.D., Eaton, J.K., 1994. Preferential concentration of heavy particles in a turbulent channel flow. Phys. Fluids 6, 3742–3749.

Février, P., Simonin, O., Squires, K.D., 2005. Partitioning of particle velocities in gas–solid turbulent flows into a continuous field and a spatially uncorrelated random distribution: theoretical formalism and numerical study. J. Fluid Mech. 533, 1–46.

Friedlander, S.K., Johnstone, H.F., 1957. Deposition of suspended particles from turbulent gas streams. Ind. Eng. Chem. Res. 49, 1151–1156.

Germano, M., Piomelli, U., Moin, P., Cabot, W.H., 1991. A dynamic subgrid-scale eddy viscosity model. Phys. Fluids 3, 1760–1765.

Grassberger, P., Procaccia, I., 1983. Measuring the strangeness of strange attractors. Physica D 9, 189–208.

Guingo, M., Minier, J.-P., 2008. A stochastic model of coherent structures for particle deposition in turbulent flows. Phys. Fluids 20, 053303.

Jimenez, J., Pinelli, A., 1999. The autonomous cycle of near-wall turbulence. J. Fluid Mech. 389, 335–359.

Kaftori, D., Hetsroni, G., Banerjee, S., 1995a. Particle behavior in the turbulent boundary layer. I. Motion, deposition, and entrainment. Phys. Fluids 7, 1095–1106.

Kaftori, D., Hetsroni, G., Banerjee, S., 1995b. Particle behavior in the turbulent boundary layer. II. Velocity and distribution profiles. Phys. Fluids 7, 1107–1121.

Kuerten, J.G.M., 2006. Subgrid modeling in particle-laden channel flow. Phys. Fluids 18, 025108.

Kuerten, J.G.M., Vreman, A.W., 2005. Can turbophoresis be predicted by large-eddy simulation? Phys. Fluids 17, 011701.

Marchioli, C., Salvetti, M.V., Soldati, A., 2008a. Some issues concerning Large-Eddy Simulation of inertial particle dispersion in turbulent bounded flows. Phys. Fluids 20, 040603.

Marchioli, C., Salvetti, M.V., Soldati, A., 2008b. Appraisal of energy recovering subgrid scale models for large-eddy simulation of turbulent dispersed flows. Acta Mech. 201, 277–296.

Marchioli, C., Soldati, A., Kuerten, J.G.M., Arcen, B., Tanière, A., Goldensoph, G., Squires, K.D., Cargnelutti, M.F., Portela, L.M., 2008c. Statistics of particle dispersion in direct numerical simulations of wall-bounded turbulence: results of an international collaborative benchmark test. Int. J. Multiphase Flow 34, 879–893.

Marchioli, C., Picciotto, M., Soldati, A., 2007. Influence of gravity and lift on particle velocity statistics and transfer rates in turbulent vertical channel flow. Int. J. Multiphase Flow 33, 227–251.

Marchioli, C., Picciotto, M., Soldati, A., 2006. Particle dispersion and wall-dependent fluid scales in turbulent bounded flow: implications for local equilibrium models. J. Turbul. 7, 1–12.

Marchioli, C., Giusti, A., Salvetti, M.V., Soldati, A., 2003. Direct numerical simulation of particle wall transfer and deposition in upward turbulent pipe flow. Int. J. Multiphase Flow 29, 1017–1038.

Marchioli, C., Soldati, A., 2002. Mechanisms for particle transfer and segregation in turbulent boundary layer. J. Fluid Mech. 468, 283–315.

Narayanan, C., Lakehal, D., Botto, L., Soldati, A., 2003. Mechanisms of particle deposition in a fully-developed turbulent open channel flow. Phys. Fluids 15, 763–775.

Niño, Y., Garcia, M.H., 1996. Experiments on particle–turbulence interactions in the near-wall region of an open channel flow: implications for sediment transport. J. Fluid Mech. 326, 285–319.

Oliemans, R.V.A., Pots, B.F.M., Trompe, N., 1986. Modeling of annular dispersed two-phase flow in vertical pipes. Int. J. Multiphase Flow 12, 711–732.

Olla, P., 2002. Transport properties of heavy particles in high Reynolds number turbulence. Phys. Fluids 14, 4266–4277.

Pan, Y., Banerjee, S., 1996. Numerical simulation of particle interactions with wall turbulence. Phys. Fluids 8, 2733–2755.

Picciotto, M., Marchioli, C., Soldati, A., 2005. Characterization of near-wall accumulation regions for inertial particles in turbulent boundary layers. Phys. Fluids 17, 098101.

Portela, L.M., Oliemans, R.V.A., 2003. Eulerian/Lagrangian DNS/LES of particle–turbulence interactions in wall-bounded flows. Int. J. Numer. Methods Fluids 43, 1045–1065.

Portela, L., Cota, P., Oliemans, R.V.A., 2002. Numerical study of the near-wall behaviour of particles in turbulent pipe flows. Powder Technol. 12, 149–157.

Reeks, M.W., 1983. The transport of discrete particles in inhomogeneous turbulence. J. Aerosol Sci. 14, 729–739.

Rouson, D.W.I., Eaton, J.K., 2001. On the preferential concentration of solid particles in turbulent channel flow. J. Fluid Mech. 428, 149–169.

Sbrizzai, F., Verzicco, R., Soldati, A., 2009. Turbulent flow and dispersion of inertial particles in a confined jet issued by a long cylindrical pipe. Flow Turbul. Combust. 82, 1–23.

Sbrizzai, F., Verzicco, R., Pidria, M., Soldati, A., 2004. Mechanisms for selective radial dispersion of microparticles in the transitional region of a confined turbulent round jet. Int. J. Multiphase Flow 30, 1389–1417.

Schoppa, W., Hussain, A.K.M.F., 2002. Coherent structure generation in near-wall turbulence. J. Fluid Mech. 453, 57–108.

Shotorban, B., Mashayek, F., 2005. Modeling of subgrid-scale effects on particles by approximate deconvolution. Phys. Fluids 17, 081701.

Shotorban, B., Zhang, K.K.Q., Mashayek, F., 2007. Improvement of particle concentration prediction in large-eddy simulation by defiltering. Int. J. Heat Mass Transfer 50, 3728–3739.

Sippola, M.R., Nazaroff, W.W., 2002. Particle deposition from turbulent flow: review of published research and its applicability to ventilation ducts in commercial buildings. Lawrence Berkeley National Laboratory Report, LBNL – 51432.

Slater, S.A., Leeming, A.D., Young, J.B., 2003. Particle deposition from two-dimensional turbulent gas flows. Int. J. Multiphase Flow 51, 275–283.

Soldati, A., 2005. Particles turbulence interactions in boundary layers. ZAMM J. Appl. Math. Mech. 85, 683–699.

Soldati, A., 2000. On the influence of electrohydrodynamics and turbulence on particle transport and collection efficiency in wire-plate electrostatic precipitators. J. Aerosol Sci. 31, 293–305.

Soldati, A., Banerjee, S., 1998. Turbulence modification by large-scale organized electrohydrodynamic flows. Phys. Fluids 10, 1742–1756.

Soldati, A., Andreussi, P., 1996. The influence of coalescence on droplet transfer in vertical annular flow. Chem. Eng. Sci. 51, 353–363.

Stolz, P., Adams, N.A., Kleiser, L., 2001. An approximate deconvolution model for large-eddy simulation with application to incompressible wall-bounded flows. Phys. Fluids 13, 997–1015.

Yeung, P.K., Pope, S.B., Sawford, B.L., 2006. Reynolds number dependence of Lagrangian statistics in large numerical simulations of isotropic turbulence. J. Turbul. 7, 1–12.

Young, J., Leeming, A., 1997. A theory of particle deposition in turbulent channel flow. J. Fluid Mech. 340, 129–159.

Please cite this article in press as: Soldati, A., Marchioli, C. Physics and modelling of turbulent particle deposition and entrainment: Review of a systematic study. Int. J. Multiphase Flow (2009), doi:10.1016/j.ijmultiphaseflow.2009.02.016